Nuclear Mathematical and Computational Sciences: A Century in Review, A Century Anew
Gatlinburg, Tennessee, April 6-11, 2003, on CD-ROM, American Nuclear Society, LaGrange Park, IL (2003)

CONVERGENCE ANALYSIS OF THE NONLINEAR COARSE MESH FINITE DIFFERENCE METHOD

Deokjung Lee and Thomas J. Downar
School of Nuclear Engineering
Purdue University
West Lafayette, IN 47907-1290 USA
lee100@ecn.purdue.edu; downar@ecn.purdue.edu

Yonghee Kim
Korea Atomic Energy Research Institute
150 Dukjin-dong, Yusong-gu, Taejon 305-353 Korea
yhkim@kaeri.re.kr

ABSTRACT

The convergence rates for the non-linear coarse mesh finite difference (CMFD) method and the coarse mesh rebalance (CMR) method are derived analytically for one-group, one-dimensional solutions of the fixed source diffusion problem in a non-multiplying infinite homogeneous medium. The derivation was performed by linearizing the non-linear algorithm and by applying Fourier error analysis to the linearized algorithm. The mesh size measured in units of the diffusion length is shown to be a dominant parameter for the convergence rate and for the stability of the iterative algorithms. Non-linear CMFD is shown to be a more effective acceleration method than CMR, especially for small mesh sizes. Both CMR and two-node CMFD algorithms are shown to be unconditionally stable. However, one-node CMFD becomes unstable for large mesh sizes. To remedy this instability, an under-relaxation of the current correction factor for the one-node CMFD method is successfully introduced and the domain of stability is significantly expanded.

Key Words: nonlinear coarse-mesh finite difference; stability; spectral radius; Fourier analysis

1. INTRODUCTION

In 1983 Kord S. Smith introduced the nonlinear coarse mesh finite difference (NCMFD) method in order to reduce the storage requirements for the analytic nodal method [1]. Since then it has become widely used to accelerate various diffusion solution methods [2-9]. More recently, NCMFD has been successfully applied to the neutron transport equations [10-12]. In principle, NCMFD is based on generalized equivalence theory (GET) [13, 14], in which discontinuity factors (DFs) are introduced to reproduce a reference higher order solution. The specific role of the DFs is to preserve the net current at the node interface such that the reaction rates in each node are preserved. NCMFD utilizes a current correction factor (CCF) in order to preserve the net current at each interface and thereby exactly reproduce a higher order solution in terms of the node-wise reaction rates and the global eigenvalue. There are no limitations in the choice of the higher order method since the CCF guarantees the equivalence between the low order coarse-mesh finite-difference (CMFD) solution and whatever the higher order solution (e.g. diffusion or transport theory, nodal or fine-mesh spatial discretization, analytic method or polynomial

expansion method, etc). Furthermore, the higher order solution can be obtained from either local one-node or two-node problems, or from a whole core solution.

The PARCS code (*P*urdue *A*dvanced *R*eactor *C*ore *S*imulator) [4, 15] has been taking advantage of the effectiveness of NCMFD accelerations. For higher order solutions, PARCS uses one-node/two-node/whole-core geometry, and has options for both the analytic nodal method (ANM) [16] and the nodal expansion method (NEM) [17, 18]. Recently a fine-mesh finite-difference (FMFD) option was introduced for either diffusion or simplified P_3 transport. For most practical LWR problems, PARCS has proven to be numerically stable for all of the solution options. However, numerical instabilities have recently been encountered for some unusual configurations. For example,

- NCMFD with a two-node local problem (NCMFD2N) solver in which large and small mesh structures are mixed randomly,

- NCMFD with a one-node local problem (NCMFD1N) solver with a very large mesh size.

The instability of the first case was reported even for a "nodal method only" without the non-linear iteration involving the CCFs [16]. It was suspected that the conventional quadratic polynomial approximation used for the transverse leakage (TL) was inadequate and was the cause for the instability. The problem was remedied by taking the differences of the mesh size into account for the TL approximation. In the second case, two remedies were investigated in which the mesh size was reduced and multiple sweeps of local one-node solutions were introduced.

Even though NCMFD has acquired considerable popularity as an acceleration technique, there has not been a methodical analysis of the stability of the NCMFD algorithm. There have been some studies on the convergence or uniqueness of the solutions of the higher order nodal method itself, especially for NEM [19-23]. But once CCFs are involved, the algorithm is non-linear and the convergence analysis becomes complicated.

In 1990 Cefus and Larsen introduced an innovative method based on Fourier analysis to analyze the stability of the non-linear CMR acceleration for the transport S_N calculation [24]. Since then, this approach has become a standard technique for the convergence analysis of non-linear acceleration methods for various transport equations [25-28]. The essential idea was to linearize the non-linear algorithm around the exact solution and then apply Fourier analysis [29, 30] to the linearized algorithm. Fourier error analysis has been the classic technique used for the stability analysis of linear methods [31-33]. For non-linear methods, the convergence rate of the linearized algorithm can be considered as the limiting value of the practical non-linear algorithm applied to the finite dimensional problem. Previous researchers have consistently reported that the numerical convergence rate in the asymptotic region of the realistic non-linear iteration compares favorably with the theoretical convergence rate of the linearized algorithm [24-26].

In this paper, we will take essentially the same approach proposed by Cefus and Larsen by linearizing and applying Fourier analysis in our study of the NCMFD algorithm. For consistency,

we will also apply the same method to the convergence analysis of the conventional partial current sweep (PCS) and the coarse mesh rebalance (CMR) algorithm used to solve the nodal diffusion equations. Finally, as a remedy for the instability of the one-node NCMFD algorithm, we will introduce a method to underrelax the CCFs.

This paper is organized as follows. The one-group, one-dimensional fixed source problem used in the analysis is introduced in section 2. Analytic convergence rates of the PCS, CMR, NCMFD1N, and NCMFD2N algorithms are derived in section 3. In section 4, performance comparisons of each acceleration method are provided which show that the theoretical approach accurately predicts the practical convergence properties. Also, it is shown in section 4 that the under-relaxation of CCF can improve the stability of the one-node NCMFD algorithm. Finally, in section 5 a non-dimensional analysis is performed and a linear version of the non-linear algorithm are introduced that provide some further insight about the basic characteristics of the various algorithms. Conclusions and continuing work are provided in section 6.

2. MODEL PROBLEM DESCRIPTION

The problem of interest here is the one-dimensional one-group diffusion problem with a flat fixed source for a non-multiplying infinite homogeneous medium. The problem can be written as:

$$-D\frac{d^2}{dx^2}\phi(x)+\Sigma\phi(x)=Q \tag{1a}$$

where

D = diffusion constant,

Σ = absorption cross section,

Q = fixed source.

The mesh structure to be used is shown in Fig. 1. A uniform mesh spacing of h will be assumed for all the iterative methods to be analyzed.

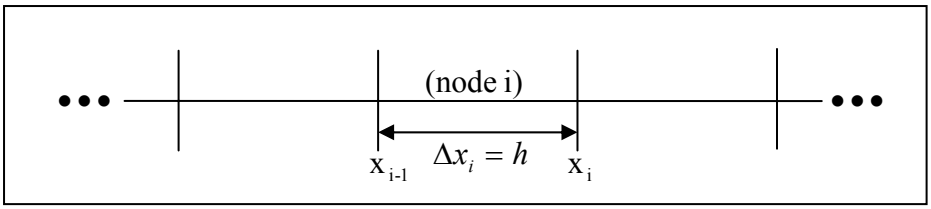

Figure 1. Mesh structure for model problem

The interface conditions are the conventional flux and current continuity:

$$\phi_i(h) = \phi_{i+1}(0) \tag{1b}$$

$$J_i(h) = J_{i+1}(0) \tag{1c}$$

where $J(x) = -D\frac{d}{dx}\phi(x)$. The parameters required to specify the problem are chosen as

- Σ_t : total cross section,
- $c\ (\equiv \Sigma_s / \Sigma_t)$: scattering ratio,
- h : mesh size.

The reason why these variables are chosen will become clear in the next section after the spectral radius of each algorithm is derived. The other quantities of interest can be expressed in terms of these parameters as:

$$\Sigma = \Sigma_t(1-c) \text{ and } D = \frac{1}{3\Sigma_t}. \tag{2}$$

For the problem of finite dimensions which will be used for the numerical evaluation of convergence rates, the mesh index i extends from 1 to N. At both boundaries, i.e., at $x = x_0$ and $x = x_N$, zero flux boundary conditions are imposed.

3. ANALYTIC DERIVATION OF CONVERGENCE RATE

For the problem described in section 2, we now derive the convergence rate of the conventional PCS method, NCMFD, and CMR acceleration methods. The centerpiece of the convergence analysis in this paper is the Fourier error analysis which provides a theoretical convergence rate for a linear iterative algorithm. Since the PCS method is linear, the Fourier analysis is directly applicable. However, for NCMFD and CMR, a linearization of the non-linear algorithm is necessary before Fourier analysis can be applied. The formulation of the spectral radius for each of the methods will be provided in the following subsections.

3.1. Partial Current Sweep

An analytic solution for node (i) in Fig. 1 can be written as:

$$\phi_i(x) = A_i \cosh(x/L) + B_i \sinh(x/L) + \frac{Q}{\Sigma} \tag{3}$$

where A_i and B_i are coefficients to be determined, and $L\ (= \sqrt{D/\Sigma})$ is the diffusion length. Two partial incoming currents at both interfaces are used to determine the coefficients A_i and B_i.

- $j_{i-1,r}^{+(k)}$: the partial current at the right interface of node (i-1) flowing in the positive x direction, i.e., the outgoing partial current from node (i-1) at the right interface, or the incoming partial current to node (i) from the left interface, at the k[th] iteration,
- $j_{i+1,l}^{-(k)}$: the partial current at the left interface of node (i+1) flowing in the negative x direction, i.e., the outgoing partial current from node (i+1) at the left interface, or the incoming partial current to node (i) at the right interface, at the k[th] iteration.

Using the analytic solution of node (i), a traditional response matrix form of the equations can be formulated as:

$$\begin{bmatrix} j_{i,l}^{-(k+1)} \\ j_{i,r}^{+(k+1)} \end{bmatrix} = \frac{1}{\chi} \begin{bmatrix} \delta_1 & \delta_2 \\ \delta_2 & \delta_1 \end{bmatrix} \begin{bmatrix} j_{i-1,r}^{+(k)} \\ j_{i+1,l}^{-(k)} \end{bmatrix} + \begin{bmatrix} d \\ d \end{bmatrix} \tag{4}$$

where

$$\delta_1 = (1 - 4L^2\Sigma^2)\sinh[h/L],\ \delta_2 = 4L\Sigma,$$
$$\chi = 4L\Sigma\cosh[h/L] + (1 + 4L^2\Sigma^2)\sinh[h/L],$$
$$d = \kappa LQ \text{, and } \kappa = 1/(\coth[h/(2L)] + 2L\Sigma).$$

The PCS algorithm is to sweep node by node updating the outgoing partial currents of each node using Eq. (4). This algorithm can be thought of as a variant of the nodal integration method for the one-group fixed source problem [34]. Let us introduce first order errors into Eq. (4), i.e., express the partial current at the k[th] iteration as a combination of exact solutions and first order error terms:

$$j_{i,l}^{-(k)} = \frac{Q}{4\Sigma}(1 + \varepsilon\xi_{i,l}^{-(k)}) \quad \text{and} \quad j_{i,r}^{+(k)} = \frac{Q}{4\Sigma}(1 + \varepsilon\xi_{i,r}^{+(k)}),\ \ \varepsilon << 1. \tag{5}$$

Inserting Eq. (5) into Eq. (4) yields:

$$\begin{bmatrix} \xi_{i,l}^{-(k+1)} \\ \xi_{i,r}^{+(k+1)} \end{bmatrix} = \frac{1}{\chi} \begin{bmatrix} \delta_1 & \delta_2 \\ \delta_2 & \delta_1 \end{bmatrix} \begin{bmatrix} \xi_{i-1,r}^{+(k)} \\ \xi_{i+1,l}^{-(k)} \end{bmatrix} \tag{6}$$

By introducing the following Fourier ansatz into Eq. (6):

$$\xi_{i,l}^{-(k)} = a_l \omega^k e^{i\lambda x_{i-1}} \quad \text{and} \quad \xi_{i,r}^{+(k)} = a_r \omega^k e^{i\lambda x_i}, \tag{7}$$

we obtain:

$$\mathbf{L}_{PCS}\,\mathbf{a} = \omega_{PCS}\,\mathbf{a} \tag{8}$$

where

$$\mathbf{L}_{PCS} = \frac{1}{\chi}\begin{pmatrix} e^{i\tau}\delta_2 & \delta_1 \\ \delta_1 & e^{-i\tau}\delta_2 \end{pmatrix}, \ \mathbf{a} = \begin{bmatrix} a_l \\ a_r \end{bmatrix}, \text{ and } \tau = \lambda h \ .$$

The matrix **L** in Eq. (8) is a function of χ, δ_1, δ_2, and τ. It is worthwhile to note that, from Eq. (4), χ, δ_1, and δ_2 are determined by ($L\Sigma$) and (h/L) which can be expressed using c and ($\Sigma_t h$) by:

$$L\Sigma = \sqrt{(1-c)/3} \quad \text{and} \quad h/L = \sqrt{3(1-c)}\Sigma_t h \,. \tag{9}$$

Therefore, the matrix **L** and a convergence rate ω is a function of τ, $\Sigma_t h$, and c:

$$\mathbf{L}_{PCS} = \mathbf{L}_{PCS}(\tau, \Sigma_t h, c) \quad \text{and} \quad \omega_{PCS} = \omega_{PCS}(\tau, \Sigma_t h, c) \,. \tag{10}$$

For a given mesh size and material properties, the convergence rate ω is a function of τ only and the spectral radius of PCS algorithm is:

$$\rho = \sup_{\tau \in [0,2\pi]} |\, \omega_{PCS}(\tau) \,| \,. \tag{11}$$

3.2. Coarse Mesh Rebalance

The CMR algorithm is one of the most common methods used to accelerate PCS. Eq. (4) can be rewritten with a new iteration index (k+1/2) instead of (k+1):

$$\begin{bmatrix} j_{i,l}^{-(k+1/2)} \\ j_{i,r}^{+(k+1/2)} \end{bmatrix} = \frac{1}{\chi}\begin{bmatrix} \delta_1 & \delta_2 \\ \delta_2 & \delta_1 \end{bmatrix}\begin{bmatrix} j_{i-1,r}^{+(k)} \\ j_{i+1,l}^{-(k)} \end{bmatrix} + \begin{bmatrix} d \\ d \end{bmatrix}. \tag{12}$$

The node average flux of node (i) consistent with Eq. (12) is

$$\overline{\phi}_i^{(k+1/2)} = \frac{Q}{\Sigma} - \frac{2\kappa}{(h/L)}\left(\frac{1}{\Sigma} + 2\right)\left(j_{i-1,r}^{+(k+1/2)} + j_{i+1,l}^{-(k+1/2)}\right). \tag{13}$$

For CMR, let us define the node average flux and the outgoing partial current of node (i) at the $(k+1)^{th}$ iteration by:

$$\overline{\phi}_i^{(k+1)} = \overline{\phi}_i^{(k+1/2)} F_i^{(k+1)}, \tag{14a}$$

$$j_{i,r}^{+(k+1)} = j_{i,r}^{+(k+1/2)} F_i^{(k+1)}, \tag{14b}$$

and

$$j_{i,l}^{-(k+1)} = j_{i,l}^{-(k+1/2)} F_i^{(k+1)} \tag{14c}$$

where the F_i's are the coarse mesh rebalance factors. By imposing the nodal balance condition for the quantities at the $(k+1)^{th}$ iteration step, we can write the CMR equation for the rebalance factors as:

$$-j_{i-1,r}^{+(k+1/2)}F_{i-1}^{(k+1)}+\left(\Sigma h\overline{\phi}_i^{(k+1/2)}+j_{i,r}^{+(k+1/2)}+j_{i,l}^{-(k+1/2)}\right)F_i^{(k+1)}-j_{i+1,l}^{-(k+1/2)}F_{i+1}^{(k+1)}=Qh \qquad (15)$$

The CMR algorithm consists of Eqs. (12), (13), (14), and (15). This method is non-linear because there is a multiplicative correction by the F_i's in Eq. (14). In order to linearize the CMR algorithm, we introduce first order error terms into the exact solution of each variable:

$$\begin{aligned}
\overline{\phi}_i^{(k+1/2)} &= \frac{Q}{\Sigma}\left(1+\varepsilon\varsigma_i^{(k+1/2)}\right)\\
F_i^{(k)} &= 1+\varepsilon f_i^{(k)}\\
j_{i,l}^{-(k)} &= \frac{Q}{4\Sigma}(1+\varepsilon\xi_{i,l}^{-(k)})\\
j_{i,r}^{+(k)} &= \frac{Q}{4\Sigma}(1+\varepsilon\xi_{i,r}^{+(k)})
\end{aligned} \qquad (16)$$

where $\varepsilon << 1$ represents a small perturbation. Inserting Eq. (16) into Eqs. (12), (13), (14), and (15), expanding in powers of ε, and dropping $O(\varepsilon^2)$ terms yields a system of linear equations in which all O(1) terms cancel each other:

$$\begin{bmatrix}\xi_{i,l}^{-(k+1/2)}\\ \xi_{i,r}^{+(k+1/2)}\end{bmatrix}=\frac{1}{\chi}\begin{bmatrix}\delta_1 & \delta_2\\ \delta_2 & \delta_1\end{bmatrix}\begin{bmatrix}\xi_{i-1,r}^{+(k)}\\ \xi_{i+1,l}^{-(k)}\end{bmatrix}, \qquad (17)$$

$$\varsigma_i^{(k+1/2)}=\frac{2\Sigma\kappa}{(h/L)}\left(\xi_{i-1,r}^{+(k)}+\xi_{i+1,l}^{-(k)}\right), \qquad (18)$$

$$\begin{aligned}
&-f_{i-1}^{(k+1)}+2(1+2\Sigma h)f_i^{(k+1)}-f_{i+1}^{(k+1)}+4\Sigma h\varsigma_i^{(k+1/2)}\\
&-\xi_{i-1,r}^{+(k+1/2)}+\xi_{i,l}^{-(k+1/2)}+\xi_{i,r}^{+(k+1/2)}-\xi_{i+1,l}^{-(k+1/2)}=0
\end{aligned}, \qquad (19)$$

and

$$\begin{aligned}
\xi_{i,r}^{+(k+1)} &= \xi_{i,r}^{+(k+1/2)}+f_i^{(k+1)}\\
\xi_{i,l}^{-(k+1)} &= \xi_{i,l}^{-(k+1/2)}+f_i^{(k+1)}
\end{aligned}. \qquad (20)$$

Fourier ansatz is then introduced as:

$$\begin{aligned}
\xi_{i,l}^{-(k)} &= a_l\omega^k e^{i\lambda x_{i-1}}\\
\xi_{i,r}^{+(k)} &= a_r\omega^k e^{i\lambda x_i}\\
\xi_{i,l}^{-(k+1/2)} &= b_l\omega^k e^{i\lambda x_{i-1}}\\
\xi_{i,r}^{+(k+1/2)} &= b_r\omega^k e^{i\lambda x_i}\\
\varsigma_i^{(k+1/2)} &= p\omega^k e^{i\lambda x_{i-1/2}}\\
f_i^{(k)} &= q\omega^k e^{i\lambda x_{i-1/2}}
\end{aligned} \qquad (21)$$

into Eqs. (17), (18), (19), and (20), which results in the linear system:

$$\mathbf{b} = \mathbf{K}\mathbf{a}, \tag{22}$$

$$p = \frac{e^{i\lambda h/2}\kappa}{(h/L)}\begin{bmatrix}1 & e^{-i\lambda h}\end{bmatrix}\mathbf{a}, \tag{23}$$

$$q = -\frac{2\Sigma h}{\mu}p + \frac{i\sin[\lambda h/2]}{\mu}\begin{bmatrix}1 & -1\end{bmatrix}\mathbf{b}, \tag{24}$$

and

$$q\begin{bmatrix}e^{ih\lambda/2}\\ e^{-ih\lambda/2}\end{bmatrix} + \mathbf{b} = \omega\ \mathbf{a} \tag{25}$$

where

$$\mathbf{a} = \begin{bmatrix}a_l\\ a_r\end{bmatrix},\ \mathbf{b} = \begin{bmatrix}b_l\\ b_r\end{bmatrix},\ \mathbf{K} = \frac{1}{\chi}\begin{bmatrix}e^{i\lambda h}\delta_2 & \delta_1\\ \delta_1 & e^{-i\lambda h}\delta_2\end{bmatrix},\ \text{and}\ \mu = 1 + 2\Sigma h - \cos[\lambda h].$$

The algebraic manipulation of Eqs. (22), (23), (24), and (25) leads to:

$$\mathbf{L}_{CMR}(\tau)\,\mathbf{a} = \omega_{CMR}(\tau)\,\mathbf{a} \tag{26}$$

where

$$\mathbf{L}_{CMR}(\tau) = \left(-\frac{2L\Sigma\kappa}{\mu}\begin{bmatrix}e^{i\tau} & 1\\ 1 & e^{-i\tau}\end{bmatrix} + \left(\frac{i\sin[\tau/2]}{\mu}\begin{bmatrix}e^{i\tau/2} & -e^{i\tau/2}\\ e^{-i\tau/2} & -e^{-i\tau/2}\end{bmatrix} + \mathbf{I}\right)\mathbf{K}\right).$$

As indicated in Eq. (26), $\mathbf{L}_{CMR}$ is a function of τ, $(L\Sigma)$, κ, and μ. Also, μ is a function of (Σh) and τ, and κ is a function of $(L\Sigma)$ and (h/L). The quantity (Σh) can be rewritten as:

$$\Sigma h = (\Sigma_t h)/(1-c)\ . \tag{27}$$

Similarly to PCS algorithm, Eqs. (9), (26), and (27) show that $\mathbf{L}_{CMR}$ and ω_{CMR} are functions of τ, $\Sigma_t h$, and c:

$$\mathbf{L}_{CMR} = \mathbf{L}_{CMR}(\tau, \Sigma_t h, c)\ \text{ and }\ \omega_{CMR} = \omega_{CMR}(\tau, \Sigma_t h, c). \tag{28}$$

For a given mesh size and material properties, the spectral radius of CMR is:

$$\rho = \sup_{\tau\in[0,2\pi]} |\,\omega_{CMR}(\tau)\,|. \tag{29}$$

A limitation of the CMR derived in this subsection is that we used the same mesh structures for both CMR and PCS, whereas in general several PCS mesh are collapsed into one coarse mesh in CMR. However, this single-mesh approach should be sufficient to capture the generic convergence properties of CMR since a more general CMR algorithm should show similar trends regarding the convergence rate.

3.3. Non-linear Coarse Mesh Finite Difference With One-Node Local Problem

The one node NCMFD algorithm NCMFD1N is characterized by the current correction factor (CCF) which is defined by

$$J_{i,l} = -\tilde{D}\left(\bar{\phi}_i - \phi_{i,l}\right) + \hat{D}_{i,l}\left(\bar{\phi}_i + \phi_{i,l}\right), \tag{30a}$$

and

$$J_{i,r} = -\tilde{D}\left(\phi_{i,r} - \bar{\phi}_i\right) + \hat{D}_{i,r}\left(\bar{\phi}_i + \phi_{i,r}\right) \tag{30b}$$

where $\tilde{D} = 2D/h$ and $\hat{D}_{i,s}$ is the CCF at the left (s=l) or right (s=r) surfaces of node (i). Note that two CCFs are defined for each node interface. Taking the corrected interface currents of Eqs. (30) into the neutron balance equation:

$$\frac{J_{i,r} - J_{i,l}}{h} + \Sigma\bar{\phi}_i = Q \tag{31}$$

provides the following CMFD equation:

$$\begin{aligned} &-\left(\frac{\tilde{D}^2 + \tilde{D}\hat{D}^{(k)}_{i-1,r} + \tilde{D}\hat{D}^{(k)}_{i,l} + \hat{D}^{(k)}_{i-1,r}\hat{D}^{(k)}_{i,l}}{2\tilde{D} - \hat{D}^{(k)}_{i-1,r} + \hat{D}^{(k)}_{i,l}}\right)\bar{\phi}^{(k)}_{i-1} - \left(\frac{\tilde{D}^2 - \tilde{D}\hat{D}^{(k)}_{i,r} - \tilde{D}\hat{D}^{(k)}_{i+1,l} + \hat{D}^{(k)}_{i,r}\hat{D}^{(k)}_{i+1,l}}{2\tilde{D} - \hat{D}_{i,r} + \hat{D}_{i+1,l}}\right)\bar{\phi}^{(k)}_{i+1} \\ &+\left(\Sigma h + \frac{\tilde{D}^2 - \tilde{D}\hat{D}^{(k)}_{i-1,r} - \tilde{D}\hat{D}^{(k)}_{i,l} + \hat{D}^{(k)}_{i-1,r}\hat{D}^{(k)}_{i,l}}{2\tilde{D} - \hat{D}^{(k)}_{i-1,r} + \hat{D}^{(k)}_{i,l}} + \frac{\tilde{D}^2 + \tilde{D}\hat{D}^{(k)}_{i,r} + \tilde{D}\hat{D}^{(k)}_{i+1,l} + \hat{D}^{(k)}_{i,r}\hat{D}^{(k)}_{i+1,l}}{2\tilde{D} - \hat{D}^{(k)}_{i,r} + \hat{D}^{(k)}_{i+1,l}}\right)\bar{\phi}^{(k)}_{i} = Qh \end{aligned} . \tag{32}$$

From the solutions of Eq. (32), the boundary conditions of 1-node problem can be constructed. The incoming partial currents at the boundaries of node (i) are

$$\begin{aligned} j^{+(k)}_{i,l} &= \frac{1}{4}\phi^{(k)}_{i,l} + \frac{1}{2}J^{(k)}_{i,l}, \\ j^{-(k)}_{i,r} &= \frac{1}{4}\phi^{(k)}_{i,r} - \frac{1}{2}J^{(k)}_{i,r}. \end{aligned} \tag{33}$$

Using these boundary conditions, the two coefficients $A_i^{(k+1/2)}$ and $B_i^{(k+1/2)}$ of the analytic solution Eq. (3) can be determined for each node (i). The node average flux ($\bar{\phi}_i^{(k+1/2)}$), surface flux ($\phi_{i,l}^{(k+1/2)}$, $\phi_{i,r}^{(k+1/2)}$) and net current ($J_{i,l}^{(k+1/2)}, J_{i,r}^{(k+1/2)}$) of higher order local solution can then be obtained and the CCFs at the (k+1/2)th step can be expressed as:

$$\hat{D}_{i,l}^{(k+1/2)} = \frac{J_{i,l}^{(k+1/2)} + \tilde{D}\left(\bar{\phi}_i^{(k+1/2)} - \phi_{i,l}^{(k+1/2)}\right)}{\bar{\phi}_i^{(k+1/2)} + \phi_{i,l}^{(k+1/2)}},$$
$$\hat{D}_{i,r}^{(k+1/2)} = \frac{J_{i,r}^{(k+1/2)} + \tilde{D}\left(\phi_{i,r}^{(k+1/2)} - \bar{\phi}_i^{(k+1/2)}\right)}{\bar{\phi}_i^{(k+1/2)} + \phi_{i,r}^{(k+1/2)}}. \tag{34}$$

As will be shown in section 4, the one-node NCMFD method is unstable for very large mesh sizes. This can be remedied by introducing a relaxation on the CCFs:

$$\hat{D}_{i,l}^{(k+1)} = \hat{D}_{i,l}^{(k)} + \alpha(\hat{D}_{i,l}^{(k+1/2)} - \hat{D}_{i,l}^{(k)}),$$
$$\hat{D}_{i,r}^{(k+1)} = \hat{D}_{i,r}^{(k)} + \alpha(\hat{D}_{i,r}^{(k+1/2)} - \hat{D}_{i,r}^{(k)}). \tag{35}$$

where α is the relaxation parameter. The range of α is (0,1] , where $\alpha = 1$ means no relaxation. The NCMFD1N algorithms are defined by Eqs. (32) through (35). In order to linearize this nonlinear algorithm, first order error perturbations are introduced into each variable

$$\bar{\phi}_i^{(k)} = \frac{Q}{\Sigma}\left(1 + \varepsilon\varsigma_i^{(k)}\right),$$
$$\hat{D}_{i,l}^{(k)} = \varepsilon\eta_{i,l}^{(k)},$$
$$\hat{D}_{i,r}^{(k)} = \varepsilon\eta_{i,r}^{(k)},$$
$$j_{i,l}^{-(k)} = \frac{Q}{4\Sigma}(1 + \varepsilon\xi_{i,l}^{-(k)}),$$
$$j_{i,r}^{+(k)} = \frac{Q}{4\Sigma}(1 + \varepsilon\xi_{i,r}^{+(k)}). \tag{36}$$

Utilizing Eq. (36) in the NCMFD1N algorithm and dropping $O(\varepsilon^2)$ terms yields a system of linear equations:

$$-\frac{\tilde{D}}{2}\varsigma_{i-1}^{(k)} + \left(h\Sigma + \tilde{D}\right)\varsigma_i^{(k)} - \frac{\tilde{D}}{2}\varsigma_{i+1}^{(k)} - \eta_{i-1,r}^{(k)} - \eta_{i,l}^{(k)} + \eta_{i,r}^{(k)} + \eta_{i+1,l}^{(k)} = 0, \tag{37}$$

$$\xi_{i,l}^{+(k)} = \left(\frac{1}{2} + \tilde{D}\right)\varsigma_{i-1}^{(k)} + \left(\frac{1}{2} - \tilde{D}\right)\varsigma_i^{(k)} + \left(2 + \frac{1}{\tilde{D}}\right)\eta_{i-1,r}^{(k)} + \left(2 - \frac{1}{\tilde{D}}\right)\eta_{i,l}^{(k)}$$
$$\xi_{i,r}^{-(k)} = \left(\frac{1}{2} - \tilde{D}\right)\varsigma_i^{(k)} + \left(\frac{1}{2} + \tilde{D}\right)\varsigma_{i+1}^{(k)} - \left(2 - \frac{1}{\tilde{D}}\right)\eta_{i,r}^{(k)} - \left(2 + \frac{1}{\tilde{D}}\right)\eta_{i+1,l}^{(k)}, \tag{38}$$

$$\begin{bmatrix}\eta_{i,l}^{(k+1/2)} \\ \eta_{i,r}^{(k+1/2)}\end{bmatrix} = \frac{1}{\chi}\begin{bmatrix}\delta_3 & -\delta_4 \\ \delta_4 & -\delta_3\end{bmatrix}\begin{bmatrix}\xi_{i,l}^{+(k)} \\ \xi_{i,r}^{-(k)}\end{bmatrix}, \tag{39}$$

and

$$\begin{aligned}\eta_{i,l}^{(k+1)} &= \eta_{i,l}^{(k)} + \alpha(\eta_{i,l}^{(k+1/2)} - \eta_{i,l}^{(k)}) \\ \eta_{i,r}^{(k+1)} &= \eta_{i,r}^{(k)} + \alpha(\eta_{i,r}^{(k+1/2)} - \eta_{i,r}^{(k)})\end{aligned}, \tag{40}$$

where

$$\begin{aligned}\delta_3 &= L\Sigma\begin{pmatrix}-(h/L)^{-2} + \left(0.5 + (h/L)^{-2} - 2(h/L)^{-2}\Sigma h\right)\cosh[h/L] \\ + \left(-(h/L)^{-1} + L\Sigma + 2(h/L)^{-2}L\Sigma\right)\sinh[h/L]\end{pmatrix}, \\ \delta_4 &= L\Sigma\left(0.5 + (h/L)^{-2}\left(-2\Sigma h - \cosh[h/L] - 2L\Sigma\sinh[h/L]\right)\right).\end{aligned}$$

The following Fourier ansatz is then used for these linearized equations:

$$\begin{aligned}\zeta_i^{(k)} &= A\omega^k e^{i\lambda x_{i-1/2}}, \\ \xi_{i,l}^{-(k)} &= b_l\omega^k e^{i\lambda x_{i-1}}, \\ \xi_{i,r}^{+(k)} &= b_r\omega^k e^{i\lambda x_i}, \\ \eta_{i,l}^{(k)} &= c_l\omega^k e^{i\lambda x_{i-1}}, \\ \eta_{i,r}^{(k)} &= c_r\omega^k e^{i\lambda x_i}, \\ \eta_{i,l}^{(k+1/2)} &= C_l\omega^k e^{i\lambda x_{i-1}}, \\ \eta_{i,r}^{(k+1/2)} &= C_r\omega^k e^{i\lambda x_i}.\end{aligned} \tag{41}$$

Inserting Eq. (41) into Eqs. (37) through (40) yields

$$A - \frac{2e^{i\tau/2}(1-e^{i\tau})}{(2e^{i\tau}\Sigma h + (1-e^{i\tau})^2\tilde{D})}\begin{bmatrix}1 & 1\end{bmatrix}\mathbf{c} = 0, \tag{42}$$

$$A\begin{bmatrix}\cos[\tau/2] - 2i\tilde{D}\sin[\tau/2] \\ \cos[\tau/2] + 2i\tilde{D}\sin[\tau/2]\end{bmatrix} + \begin{bmatrix}+2 - 1/\tilde{D} & +2 + 1/\tilde{D} \\ -2 - 1/\tilde{D} & -2 + 1/\tilde{D}\end{bmatrix}\mathbf{c} - \mathbf{b} = 0, \tag{43}$$

$$\mathbf{C} - \frac{1}{\chi}\begin{bmatrix}\delta_3 & -e^{i\tau}\delta_4 \\ e^{-i\tau}\delta_4 & -\delta_3\end{bmatrix}\mathbf{b} = 0, \tag{44}$$

and

$$\omega\,\mathbf{c} = (1-\alpha)\,\mathbf{c} + \alpha\,\mathbf{C}. \tag{45}$$

where

$$\mathbf{b} = \begin{bmatrix}b_l \\ b_r\end{bmatrix},\ \mathbf{c} = \begin{bmatrix}c_l \\ c_r\end{bmatrix},\ \text{and}\ \mathbf{C} = \begin{bmatrix}C_l \\ C_r\end{bmatrix}.$$

The algebraic manipulation of Eqs. (42) through (45) leads to:

$$\mathbf{L}_{NCMFD1N}\,\mathbf{c} = \omega_{NCMFD1N}\,\mathbf{c} \tag{46}$$

where

$$\mathbf{L}_{NCMFD1N} = (1-\alpha)\mathbf{I} + \alpha\mathbf{H},$$

$$\mathbf{H} = -\frac{1}{\chi}\begin{bmatrix} \delta_3 & -e^{i\tau}\delta_4 \\ e^{-i\tau}\delta_4 & -\delta_3 \end{bmatrix}\left(\frac{e^{i\tau/2}\Sigma h(1-e^{i\tau})}{(e^{i\tau}(\Sigma h)^2 + (1-e^{i\tau})^2)} \begin{bmatrix} \cos[\tau/2] - 4i\sin[\tau/2]/(3\Sigma h) \\ \cos[\tau/2] + 4i\sin[\tau/2]/(3\Sigma h) \end{bmatrix} [1 \quad 1] + \begin{bmatrix} +2-1.5\Sigma h & +2+1.5\Sigma h \\ -2-1.5\Sigma h & -2+1.5\Sigma h) \end{bmatrix} \right).$$

By inspection of the matrix **H**, it is apparent that the matrix $\mathbf{L}_{NCMFD1N}$ is a function of $(\tau, \Sigma h, c, \alpha)$ and therefore $\omega_{NCMFD1N}$ is also a function of $(\tau, \Sigma h, c, \alpha)$:

$$\mathbf{L}_{NCMFD1N} = \mathbf{L}_{NCMFD1N}(\tau, \Sigma_t h, c, \alpha) \quad \text{and} \quad \omega_{NCMFD1N} = \omega_{NCMFD1N}(\tau, \Sigma_t h, c, \alpha) \tag{47}$$

The convergence rate of NCMFD1N can then be expressed as:

$$\rho = \sup_{\tau\in[0,2\pi]} |\,\omega_{NCMFD1N}(\tau)\,|. \tag{48}$$

3.4. Non-linear Coarse Mesh Finite Difference With 2-Node Local Problem

The two-node NCMFD algorithm NCMFD2N is characterized by the CCF which is defined by:

$$J_{i,i+1} = -\tilde{D}\left(\bar{\phi}_{i+1} - \bar{\phi}_i\right) + \hat{D}_{i,i+1}\left(\bar{\phi}_{i+1} + \bar{\phi}_i\right) \tag{49}$$

where $\tilde{D} = D/h$ and $\hat{D}_{i,i+1}$ is the CCF at the interface of node (i) and (i+1). Incorporating the corrected net current at node interface, Eq. (49), with the nodal balance, Eq. (31), leads us to the CMFD equation:

$$-\left(\tilde{D} + \hat{D}^{(k)}_{i-1,i}\right)\bar{\phi}^{(k)}_{i-1} + \left(\Sigma h + (2\tilde{D} + \hat{D}^{(k)}_{i-1,i} + \hat{D}^{(k)}_{i,i+1})\right)\bar{\phi}^{(k)}_{i} - \left(\tilde{D} - \hat{D}^{(k)}_{i,i+1}\right)\bar{\phi}^{(k)}_{i+1} = Qh \tag{50}$$

In order to update CCFs, the NCMFD2N algorithm solves local problems consisting of the adjacent two nodes per interface. In the local problem, the unknowns are the four coefficients $A_i^{(k+1)}$, $B_i^{(k+1)}$, $A_{i+1}^{(k+1)}$, and $B_{i+1}^{(k+1)}$ of the higher order solutions in the form of Eq. (3) in both nodes (i) and (i+1). Flux continuity and current continuity at the interface and node average fluxes in both nodes are used to determine those unknowns in a local problem:

$$\phi^{(k+1)}_i(h) = \phi^{(k+1)}_{i+1}(0) \tag{51a}$$

$$J^{(k+1)}_i(h) = J^{(k+1)}_{i+1}(0) \tag{51b}$$

$$\bar{\phi}^{(k)}_i = \frac{1}{h}\int_{\Delta x_i} \phi^{(k+1)}_i(x)dx \tag{51c}$$

$$\bar{\phi}^{(k)}_{i+1} = \frac{1}{h}\int_{\Delta x_{i+1}} \phi^{(k+1)}_{i+1}(x)dx \tag{51d}$$

From the solution of local problems, the higher order net current at the interface is obtained:

$$J_{i,i+1}^{(k+1)} = -\frac{\Sigma h}{4}\mathrm{csch}[h/(2L)]^2(\bar{\phi}_{i+1}^{(k)} - \bar{\phi}_i^{(k)}). \tag{52}$$

And the CCF is updated by:

$$\hat{D}_{i,i+1}^{(k+1)} = \frac{J_{i,i+1}^{(k+1)} + \tilde{D}\left(\bar{\phi}_{i+1}^{(k)} - \bar{\phi}_i^{(k)}\right)}{\bar{\phi}_i^{(k)} + \bar{\phi}_{i+1}^{(k)}}. \tag{53}$$

NCMFD2N algorithms are defined by Eqs. (50), (52), and (53). Introducing the following first order perturbations

$$\begin{aligned} \bar{\phi}_i^{(k)} &= \frac{Q}{\Sigma}\left(1+\varepsilon\varsigma_i^{(k)}\right), \\ \hat{D}_{i,i+1}^{(k)} &= \varepsilon\eta_{i,i+1}^{(k)}. \end{aligned} \tag{54}$$

into the NCMFD2N algorithms, which leads to a set of linearized equations:

$$-\tilde{D}\varsigma_{i-1}^{(k)} + (\Sigma h + 2\tilde{D})\varsigma_i^{(k)} - \tilde{D}\varsigma_{i+1}^{(k)} - 2\eta_{i-1,i}^{(k)} + 2\eta_{i,i+1}^{(k)} = 0, \tag{55}$$

$$\Sigma h(1+2(h/L)^{-2}(1-\cosh[h/L]))\mathrm{csch}[h/(2L)]^2(\varsigma_{i+1}^{(k)} - \varsigma_i^{(k)}) + 8\eta_{i,i+1}^{(k+1)} = 0. \tag{56}$$

The following Fourier ansatz:

$$\begin{aligned} \zeta_i^{(k)} &= a\omega^k e^{i\lambda x_{i-1/2}} \\ \eta_{i,i+1}^{(k)} &= b\omega^k e^{i\lambda x_i} \end{aligned} \tag{57}$$

is appropriate for the analysis of the linearized algorithm Eqs. (55) and (56), which lead to:

$$a(\Sigma h + 2(1-\tilde{D}\cos[\lambda h])) + 4ib\sin[\lambda h/2] = 0 \tag{58}$$

$$4\omega b + ai\Sigma h(1+2(h/L)^{-2}(1-\cosh[h/L]))\mathrm{csch}[h/(2L)]^2\sin[\lambda h/2] = 0 \tag{59}$$

From Eqs. (58) and (59), the convergence rate of NCMFD2N is:

$$\omega_{NCMFD2N} = \frac{(2+3(1-c)(\Sigma_t h)^2 - 2\cosh[\sqrt{3(1-c)}\Sigma_t h)\mathrm{csch}[\sqrt{3(1-c)}\Sigma_t h/2]^2\sin[\tau/2]^2}{2+3(1-c)(\Sigma_t h)^2 + 2\cos[\tau]} \tag{60}$$

and the spectral radius is:

$$\rho = \sup_{\tau\in[0,2\pi]} |\omega_{NCMFD2N}(\tau, \Sigma_t h, c)|. \tag{61}$$

3.5. Spectral Radius

In the previous sections, the analytic prescriptions were derived for the convergence rates of the four algorithms: PCS, CMR, NCMFD1N, and NCMFD2N. For the NCMFD2N algorithm, the convergence rate is explicitly given by Eq. (60). But for PCS, CMR, and NCMFD1N, the convergence rates are given implicitly as eigenvalues of the 2x2 matrix **L** representing each algorithm as in Eqs. (8), (26), and (46). If the matrix **L** is defined by:

$$\mathbf{L} = \begin{bmatrix} l_{11} & l_{12} \\ l_{21} & l_{22} \end{bmatrix}, \tag{62}$$

then the spectral radius of an algorithm expressed by the matrix **L** can be expressed explicitly as:

$$\rho = Max\left[\begin{array}{l} \left|(l_{11}+l_{22}-\sqrt{l_{11}^2+4l_{12}l_{21}-2l_{11}l_{22}+l_{22}^2})/2\right|, \\ \left|(l_{11}+l_{22}+\sqrt{l_{11}^2+4l_{12}l_{21}-2l_{11}l_{22}+l_{22}^2})/2\right| \end{array}\right]. \tag{63}$$

Therefore, the spectral radius for the four algorithms considered in this paper can be determined as long as $\Sigma_t h$ and c are specified. In Fig. 2, the convergence rates are plotted as a function of $\tau(=\lambda h)$ for each algorithm.

The slowest convergence rates occur at $\tau=0$ for PCS, CMR, and NCMFD1N, but at $\tau=\pi$ for NCMFD2N. Therefore, the spectral radius of each algorithm can be expressed as:

$$\rho = |\,\omega_M(\tau_0, \Sigma_t h, c)\,| \tag{64}$$

where $\tau_0=0$ for M=PCS, CMR, and NCMFD1N and $\tau_0=\pi$ for M=NCMFD2N. With all other conditions fixed, a higher scattering ratio implies a smaller absorption cross section. This explains the case of c=0.95 which shows slower convergence than c=0.9 for PCS and CMR. However, this is not the case for NCMFD1N and NCMFD2N where it is observed that a higher scattering ratio provides the fastest convergence rate. As will be shown in the non-dimensional analysis of section 6, a higher scattering ratio corresponds to a smaller mesh size in non-dimensional units. As will be seen in the next section (Fig. 4), the rate of convergence is faster for smaller optical mesh sizes ($\Sigma_t h$).

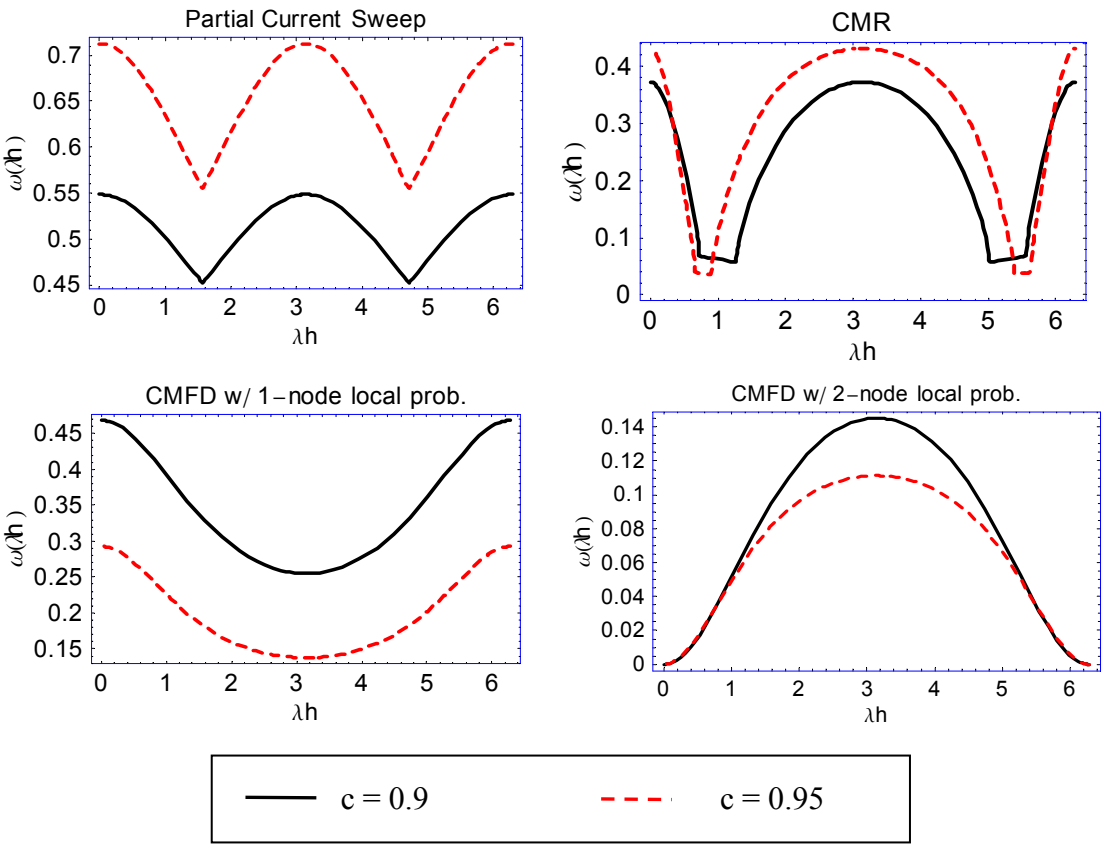

Figure 2. Convergence rate vs. frequency of error mode

4. NUMERICAL RESULTS

For the model problem described in section 2, additional insight can be provided by assigning realistic one-group LWR data for the cross sections and mesh size. The data used here are listed in Table I and were taken from a OECD NEACRP LWR benchmark problem and collapsed using a fast to thermal flux ratio of 6. The data noted as A are adequate to fully specify the problem, and the data noted as B are derived from data A for the numerical evaluation of the spectral radius. Also, for purposed of evaluating the numerical spectral radius, a finite dimension problem is considered with the total number of mesh as 40 and with zero flux boundary conditions.

For a finite dimensional problem with flux zero boundary conditions, the four algorithms under consideration were implemented and the numerical spectral radius was evaluated using:

$$\rho_{num} = \frac{\left\| \boldsymbol{\varphi}^{(k)} - \boldsymbol{\varphi}^{(k-1)} \right\|_2}{\left\| \boldsymbol{\varphi}^{(k-1)} - \boldsymbol{\varphi}^{(k-2)} \right\|_2} \tag{64}$$

where $\boldsymbol{\varphi}^{(k)}$ is a vector of node average fluxes at the k^{th} iteration. In Fig. 3, the numerical spectral radius of the NCMFD1N algorithm with the problem data in Table I, is plotted as a function of the number of mesh. As shown in the Figure, ρ_{num} becomes asymptotic after about 20 mesh. Therefore, the number of mesh was fixed at 40 for the numerical analysis of the five algorithms.

Table I. Model Problem Data

Data Set A	Abs. c.x. Σ (cm^{-1})	0.02
	Scattering ratio c [1)]	0.95
	Mesh size h (cm)	10
Data Set B (Derived from data A)	Total c.x. Σ_t [2)] (cm^{-1})	0.40
	Diffusion constant D [3)] (cm)	0.8333
	Optical mesh size $\Sigma_t h$	4.0
Geometric Data	Number of mesh	40
	Boundary condition	Zero Flux

1) $c \equiv \Sigma_s / \Sigma_t$

2) $\Sigma_t = \Sigma / (1 - c)$

3) $D = 1/(3\Sigma_t)$

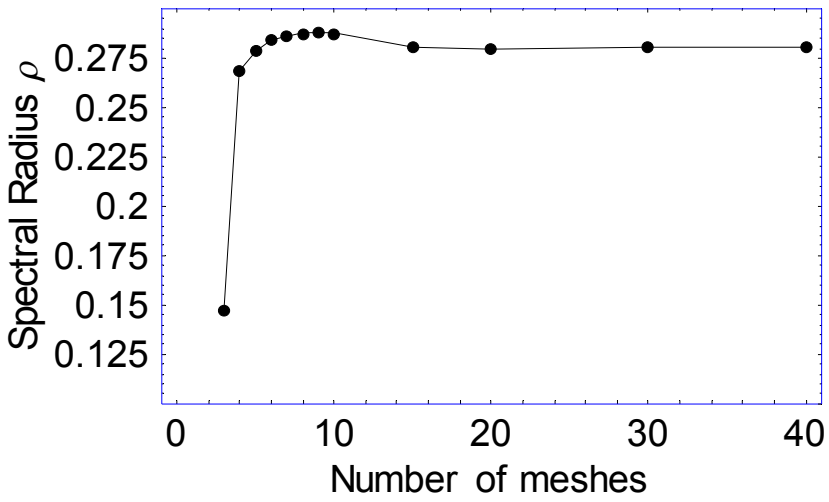

Figure 3. Numerical Spectral Radius vs. Number of Mesh

(CMFD w/ 1-node local prob.)

In Fig. 4, the theoretical and numerical results of ρ versus $\Sigma_t h$ are plotted for each method. This figure demonstrates the excellent agreement of theoretical and experimental values for all the methods. For PCS and CMR, the spectral radius becomes unity as the mesh size approaches zero and becomes asymptotic at a value less than unity as the mesh size goes to infinity. In particular, it is seen that the CMR algorithm has an optimum value of mesh size from the convergence point of view. The spectral radius of the CMFD algorithms tends to zero as mesh size becomes smaller. PCS, CMR, and NCMFD2N algorithms are always stable, however the NCMFD1N algorithm becomes unstable for a large mesh sizes.

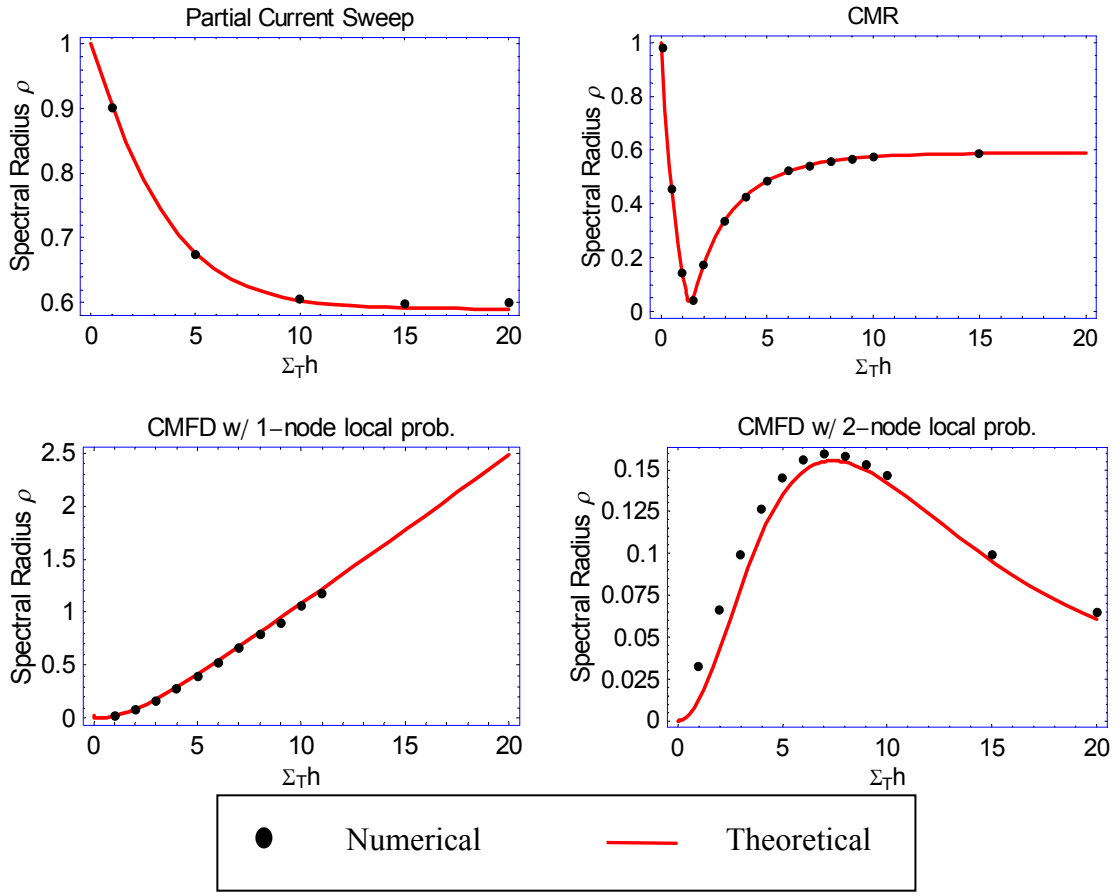

Figure 4. Spectral Radius vs. $\Sigma_t h$ (c=0.95)

Fig. 5 demonstrates the importance of the scattering ratio on the spectral radius for each method. The net effect of increasing the scattering ratio with all the other quantities fixed is equivalent to reducing the absorption cross section. As expected, increasing the scattering ratio leads to a negative effect (reduces the rate of convergence) for PCS and CMR. As noted at the end of section 3, the larger scattering ratio yields a smaller non-dimensional mesh size for the NCMFD1N and NCMFD2D algorithms, which shifts the plot of spectral radius versus ($\Sigma_t h$) in the positive x- axis direction as shown in Fig. 5.

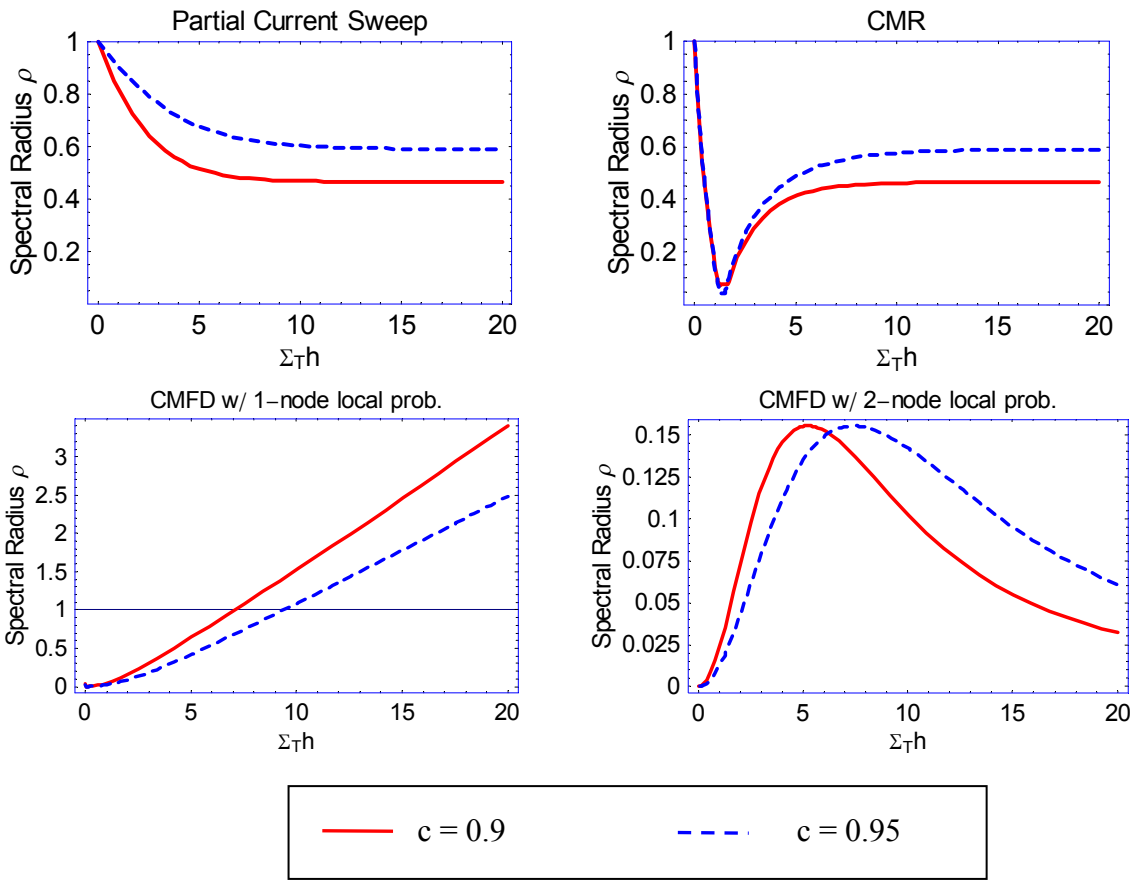

Figure 5. Spectral Radius vs. $\Sigma_t h$ for Different Scattering Ratios

In Fig. 6, the spectral radius of NCMFD1N versus the relaxation parameter α is plotted for different mesh sizes. (Note: $\alpha = 1$ indicates no relaxation). For no relaxation, the spectral radius increases as the mesh size becomes larger and eventually it becomes greater than unity, i.e., the algorithm becomes unstable (e.g, for a mesh size of 50 cm, the spectral radius is 2.5). However, even in this case the application of under-relaxation can bring the algorithm back into a stable region, as shown in the Figure. Also apparent in Figure 6, is that there appears to be an optimum value of under-relaxation parameters depending on the mesh size (i.e. the larger the mesh size, the more under-relaxation is required). Another fact worthwhile noting in the Figure is that the over-relaxation ($\alpha > 1$) always reduces the rate of convergence.

In Fig. 7, the spectral radius of NCMFD1N versus ($\Sigma_t h$) is plotted for different relaxation parameters. With no relaxation, the region of stability is ($\Sigma_t h$) < 10. However, as more under-relaxation is applied, the region of stability is further expanded (e.g. for the relaxation parameter $\alpha = 0.3$, the stability region is four times larger than with no relaxation). Although we can expand the stability region, under-relaxation has the adverse effect of increasing the spectral radius for problems with a small mesh size.

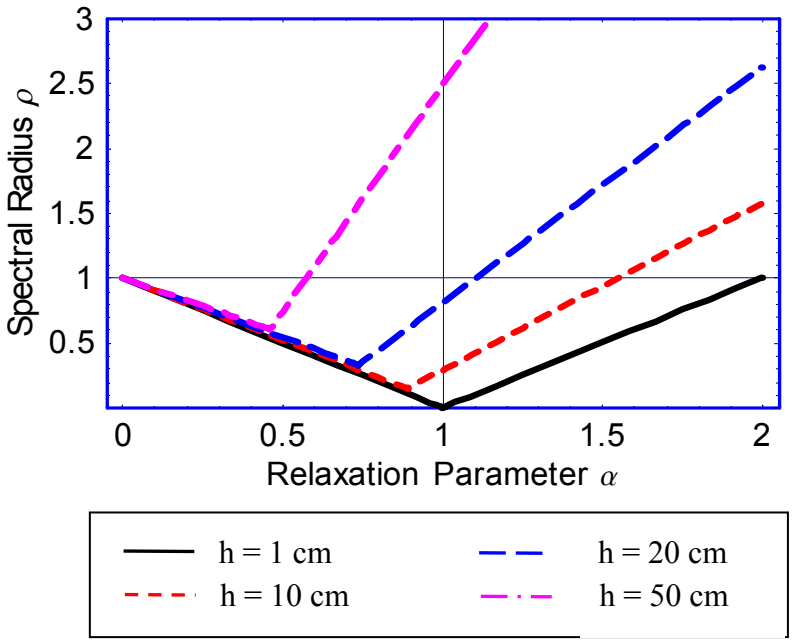

Figure 6. Spectral radius of CMFD w/ 1-node local prob. vs. relaxation parameter

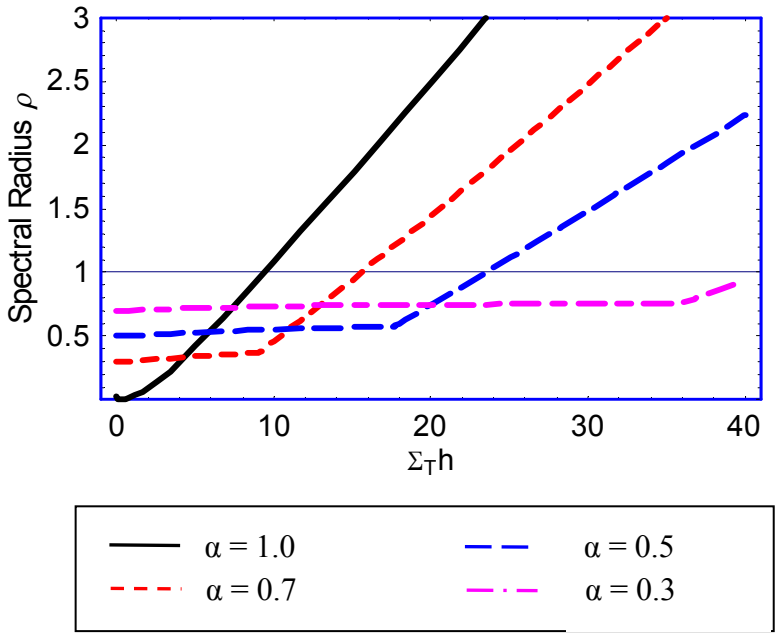

Figure 7. Sensitivity to relaxation parameter α of the spectral radius of "CMFD w/ 1-node local prob."

In Fig. 8, the spectral radius is plotted versus ($\Sigma_t h$) for each of the five iterative strategies examined here. For the case given in Table I, i.e., $\Sigma_t h = 4$, both CMR and CMFD effectively accelerate PCS. As the mesh size becomes smaller, CMFD acceleration becomes more effective compared with CMR. For large mesh sizes, NCMFD2N is still more effective than CMR. However NCMFD1N becomes unstable and even the under-relaxed NCMFD1N is only comparable to CMR. Overall, NCMFD2N shows better performance than CMR in terms of the convergence rate. It should be noted that CMR is comparable to CMFD only for a very short range of ($\Sigma_t h$) around its optimum value. For large mesh sizes, CMR and NCMFD1N are comparable to PCS in terms of the convergence rate.

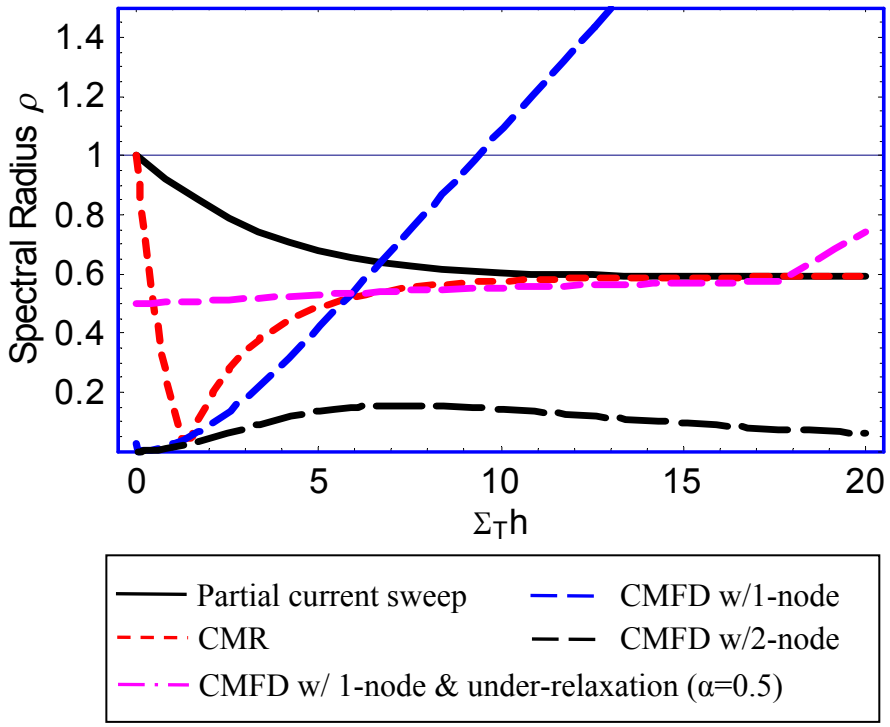

Figure 8. Spectral radius depending on iteration method

5. ANALYSIS

In this section, a non-dimensional analysis and a linear version of the non-linear algorithm are introduced that provide some additional insight about the basic characteristics of the various algorithms.

5.1. Non-dimensional Analysis

In order to understand the most dominant parameters determining the characteristics of the model problem, a non-dimensional analysis can be performed for the model problem defined by Eqs. (1). Introducing non-dimensional quantities:

$$x^* = x / L \tag{65a}$$

$$\phi^* = \frac{\phi}{Q/\Sigma} \tag{65b}$$

$$J^* = \frac{J}{LQ} \tag{65c}$$

into Eqs. (1) leads to:

$$-\frac{d^2}{dx^{*2}}\phi^*(x^*) + \phi^*(x^*) = 1 \tag{66}$$

with the interface conditions:

$$\phi_i^*(h^*) = \phi_{i+1}^*(0) \tag{67a}$$

$$J_i^*(h^*) = J_{i+1}^*(0) \tag{67b}$$

where $J^*(x^*) = -\frac{d}{dx^*}\phi^*(x^*)$. From Eqs. (66) and (67), it is clear that the non-dimensional mesh size h^* *(=h/L)* is the only parameter required to specify the problem completely. Therefore, for any numerical method applied to solve the non-dimensional system of equations, the convergence properties, as well as the solution itself will be uniquely determined by h^*. Using the definition of the diffusion length and Eq. (2), h^* can be rewritten as in Eq. (9):

$$h^* = \sqrt{3(1-c)}\left(\Sigma_t h\right) \tag{68}$$

The non-dimensional mesh size h^* is determined by the scattering ratio c and the optical mesh size ($\Sigma_t h$), which is consistent with the theoretical derivation of the spectral radius in section 3.

5.2. Linear Version of NCMFD2N Algorithm

The two-node NCMFD algorithm is a non-linear procedure in which the non-linearity is introduced from the definition of the CCFs in Eq. (49). A linear CMFD with a two-node local problem (LCMFD2N) can be formulated by using a slightly different definition of the CCF. Specifically, if the CCF is written as:

$$J_{i,i+1} = -\tilde{D}\left(\bar{\phi}_{i+1} - \bar{\phi}_i\right) + \frac{2Q}{\Sigma}\hat{D}_{i,i+1} \tag{69}$$

where $\hat{D}_{i,i+1}$ is CCF, then the nodal balance equation can be written as:

$$-\left(\tilde{D}\right)\bar{\phi}_{i-1}^{(k)}+\left(\Sigma h+2\tilde{D}\right)\bar{\phi}_{i}^{(k)}-\left(\tilde{D}\right)\bar{\phi}_{i+1}^{(k)}=Qh+\left(2Q/\Sigma\right)\left(\hat{D}_{i-1,i}^{(k)}-\hat{D}_{i,i+1}^{(k)}\right) \tag{70}$$

The CCF is then updated using higher order interface currents of Eq. (52) as:

$$\hat{D}_{i,i+1}^{(k+1)}=\frac{J_{i,i+1}^{(k+1)}+\tilde{D}\left(\bar{\phi}_{i+1}^{(k)}-\bar{\phi}_{i}^{(k)}\right)}{2Q/\Sigma}. \tag{71}$$

Inserting Eq. (52) into Eq. (71) yields:

$$\Sigma h(1+2(h/L)^{-2}(1-\cosh[h/L]))\mathrm{csch}[h/(2L)]^{2}\left(\bar{\phi}_{i+1}^{(k)}-\bar{\phi}_{i}^{(k)}\right)+8(Q/\Sigma)\hat{D}_{i,i+1}^{(k+1)}=0. \tag{72}$$

The LCMFD2N algorithm consists of Eqs. (70) and (72). The convergence rate of LCMFD2N will be exactly the same as the linearized NCMFD2D since the LCMFD2N algorithm, Eqs. (70) and (72), can be converted into the linearized NCMFD2N, Eqs. (55) and (56), by the following linear transformation :

$$\begin{bmatrix}\varsigma_{i}^{(k)}\\ \eta_{i,i+1}^{(k)}\end{bmatrix}=\begin{bmatrix}\Sigma/Q & 0\\ 0 & 1\end{bmatrix}\begin{bmatrix}\bar{\phi}_{i}^{(k)}\\ \hat{D}_{i,i+1}^{(k)}\end{bmatrix}-\begin{bmatrix}1\\ 0\end{bmatrix} \tag{73}$$

The linear CMR algorithm and the linear CMFD method for the one-node local problem can be constructed in a similar manner for the model problem.

6. CONCLUSIONS

For the one-group diffusion fixed source problem, we have performed theoretical studies on the convergence rates of the PCS, CMR, and NCMFD iterative methods. PCS, CMR, NCMFD1N, and NCMFD2N algorithms were constructed for a model problem and the non-linear algorithms of CMR and NCMFD were linearized for Fourier analysis. Fourier error analysis was then applied to each method and the convergence rates were derived analytically. The numerical spectral radius of each method was evaluated for the model problem with a finite number of mesh. Non-dimensional equations were then formulated for the model problem and the dominant factors affecting the rate of convergence were identified. A linear version of the CMFD algorithm with a 2-node local problem was also formulated. Finally, an under-relaxation was applied to mitigate the instability of the NCMFD1N algorithm.

Some of the conclusions of this study can be summarized as follows:

- The method proposed by Cefus and Larsen to apply Fourier analysis to the linearized equations effectively predicts the convergence rates of nonlinear methods in the vicinity of the exact solutions.

- The theoretical and experimental convergence rates agree well with each other, and the theoretical spectral radius provides a limiting value of the numerical convergence rate.

- The convergence rates are dependent only on the error mode frequency τ, the optical mesh size ($\Sigma_t h$), and the scattering ratio c. The convergence rate of the NCMFD1N with under-relaxation also depends on the relaxation parameter α.

- The PCS, CMR, and NCMFD2N algorithms are always stable. However, the NCMFD1N algorithm becomes unstable for large mesh sizes.

- The stability domain of NCMFD1N can be expanded substantially by under-relaxation.

- Each iterative method has its own value of the error mode frequency τ_0, which gives the slowest convergence rate, i.e., the spectral radius.

- The NCMFD2N algorithm has a corresponding linear algorithm LCMFD2N which is equivalent to the linearized NCMFD2N in terms of convergence rate. This is expected to be true for the other non-linear methods, CMR and NCMFD1N.

- Non-dimensional analysis reveals that the only control parameter of the model problem is the non-dimensional mesh size scaled on the diffusion length, which is a function of the scattering ratio c and ($\Sigma_t h$).

- NCMFD accelerates PCS more effectively than CMR, especially for problems with small mesh size.

In summary, the study here provides a robust and reliable method to analyze the stability and rate of convergence for the CMR and NCMFD methods used as an acceleration of PCS. Further work is ongoing to extend this analysis to multi-group, multi-dimensional problems.

ACKNOWLEDGMENTS

The authors wish to acknowledge the support for this work provided by the Department of Energy NEER program and by the United States Regulatory Commission.

REFERENCES

1. K. S. Smith, “Nodal Method Storage Reduction by Non-linear Iteration,” *Trans. Am. Nucl. Soc.*, **44**, 265 (1983).
2. J. M. Aragones and C. Ahnert, “A Linear Discontinuous Finite Difference Formulation for Synthetic Coarse-Mesh Few-Group Diffusion Calculation,” *Nucl. Sci. Eng.*, **94**, p.309 (1986).
3. P. R. Engrand, G. I. Maldonado, R. Al-Chalabi and P. J. Turinsky, “Non-linear Iteration Strategy for NEM: Refinement and Extension,” *Trans. Am. Nucl. Soc.*, **65**, p.221 (1992).

4. H. G. Joo, D. A. Barber, G. Jiang, and T. J. Downar, *PARCS: A Multi-Dimensional Two-Group Reactor Kinetics Code Based on the Nonlinear Analytic Nodal Method*, PU/NE-98-26, Purdue University, 1998.
5. Kap Suk Moon, Nam Zin Cho, Jae Man Noh, and Ser Gi Hong, "Acceleration of the Analytic Function Expansion Nodal Method by Two-Factor Two-Node Nonlinear Iteration," *Nucl. Sci. Eng.*, **132**, pp.194-202 (1999).
6. H. C. Shin, Y. H. Kim, and Y. B. Kim, "One-Node Coarse-Mesh Finite Difference Algorithm for Fine-Mesh Finite Difference Operator," *Trans. Am. Nucl. Soc.*, **81**, p.150 (1999).
7. Y. A. Chao, "A Theoretical Analysis of the Coarse Mesh Finite Difference Representation in Advanced Nodal Method," *Proc. M&C'99-Madrid, Mathematics and Computation, Reactor Physics and Environmental Analysis in Nuclear Application,* **Vol. 1**, pp. 117-126, Madrid, Spain, September 27-30 (1999).
8. Y. A. Chao, "Coarse Mesh Finite Difference Methods and Applications," *Proc. ANS Int. Top. Meeting on Advances in Reactor Physics and Mathematics and Computation into the Next Millenium, 9404, PHYSOR 2000,* Pittsburgh PA, USA, May 7-12 (2000).
9. Nuria Garcia-Herranz, O. Cabellos, J. M. Aragones, and C. Ahnert, "Performance of the Analytic Coarse Mesh Finite Difference Method With Heterogeneous Nodes," *Proc. ANS Reactor Physics Topical Meeting, PHYSOR 2002,* Seoul, Korea, October 7-10 (2002).
10. C. Lee and T. J. Downar, "Non-linear Formulation for Multi-group Simplified P3," *Trans. Am. Nucl. Soc.*, **83**, p.297 (2000).
11. K. S. Smith and J. D. Rhodes, III, "Full-Core, 2-D, LWR Core Calculations with CASMO-4E," *Proc. ANS Reactor Physics Topical Meeting, PHYSOR 2002,* Seoul, Korea, October 7-10 (2002).
12. H. G. Joo, J. Y. Cho, H. Y. Kim, S. Q. Zee, and M. H. Chang, "Dynamic Implementation of the Equivalence Theory in the Heterogeneous Whole Core Transport Calculation," *Proc. ANS Reactor Physics Topical Meeting, PHYSOR 2002,* Seoul, Korea, October 7-10 (2002).
13. K. S. Smith, *Spatial Homogenization Methods for Light Water Reactors*, Thesis, Department of Nuclear Engineering, Mass. Inst. Of Tech., Cambridge, MA. (1980).
14. K. S. Smith, "Assembly Homogenization Techniques for Light Water Reactor Analysis," *Prog. Nucl. Energy*, **17**, pp.303-335 (1986).
15. T. J. Downar, et. al., "PARCS: Purdue Advanced Reactor Core Simulator," *Proc. ANS Reactor Physics Topical Meeting, PHYSOR 2002,* Seoul, Korea, October 7-10 (2002).
16. K. S. Smith, *An Analytic Nodal Method for Solving the 2-Group, Multi-Dimensional, Static and Transient Neutron Diffusion Equations*, Thesis, Department of Nuclear Engineering, Mass. Inst. of Tech., Cambridge, MA. (1979).
17. H. Finnemann, F. Bennewitz, and M. R. Wagner "Interface Current Technique for Multidimensional Reactor Calculations," *Atomkernergie*, **30**, pp.123-128 (1977).
18. R. D. Lawrence, "Progress In Nodal Methods For the Solution of the Neutron Diffusion and Transport Equations," *Prog. Nucl. Energy*, **17**, pp.271-301 (1986).
19. R. S. Modak and S. B. Degweker, "Convergence Of The Iteration Scheme In The Nodal Expansion Method For The Solution Of The Diffusion Equation," *Ann. Nucl. Energy*, **13**, pp.539-543 (1986).
20. R. C. Penland, Y. Y. Azmy, and P. J. Turinsky, "Error Analysis of the Nodal Expansion Method for Solving the Neutron Diffusion Equation," *Nucl. Sci. Eng.*, **125**, pp.284-299 (1997).

21. M. R. Zika and T. J. Downar, "Numerical Divergence Effects of Equivalence Theory in the Nodal Expansion Method," *Nucl. Sci. Eng.*, **115**, pp.219-232 (1993).
22. C. J. Hah and T. J. Downar, "An Augmented Source Method for the Application of Nodal Equivalence Theory," *Nucl. Sci. Eng.*, **121**, pp.405-415 (1995).
23. W. S. Yang, "Response Matrix Properties and Convergence Implications for an Interface-Current Nodal Formulation," *Nucl. Sci. Eng.*, **121**, pp.416-432 (1995).
24. G.regory R. Cefus and Edward W. Larsen, "Stability Analysis of Coarse-Mesh Rebalance," *Nucl. Sci. Eng.*, **105**, pp.31-39 (1990).
25. Bingjing Su, Michael G. Fired, and Edward W. Larsen, "Stability Analysis of The Variable Eddington Factor Method," *Transport Theory Statist. Phys.*, **30(4-6)**, pp.439-455 (2001).
26. Gregory R. Cefus and Edward W. Larsen, "Stability Analysis of The Quasidiffusion and Second Moment Methods For Iteratively Solving Discrete-Ordinates Problems," *Transport Theory Statist. Phys.*, **18(5&6)**, pp.493-511 (1989-1990).
27. Ser Gi Hong and Nam Zin Cho, "Convergence Analysis of the Angular-Dependent Rebalance Iteration Method in X-Y Geometry," *Trans. Am. Nucl. Soc.*, **80**, p.115 (1999).
28. Chang Je Park and Nam Zin Cho, "Additive Angular Dependent Rebalance with Extrapolation for Discrete Ordinates Transport Equation," *Trans. Am. Nucl. Soc.*, **86**, p.208 (2002).
29. R. D. Richtmeyer, *Difference Methods for Initial-Value Problems*, New York University, New York, USA (1957).
30. R. J. LeVeque, "Finite Difference Methods for Differential Equations," AMath 585-6 Course Notes, University of Washington, http://www.amath.washington.edu/courses/585-winter-2001/585-6.ps.z (2002).
31. Edward W. Larsen, "Unconditionally Stable Diffusion-Synthetic Acceleration Methods for the Slab Geometry Discrete Ordinates Equations. Part I: Theory," *Nucl. Sci. Eng.*, **82**, pp.47-63 (1982).
32. Chang Je Park, *Higher-Order Difference Method for Solving the Neutron Diffusion and Transport Equation*, Thesis, Department of Nuclear Engineering, Korea Advanced Institute of Science and Technology (2001).
33. Marvin L. Adams and Edward W. Larsen, "Fast Iterative Methods For Discrete-Ordinates Particle Transport Calculations," *Prog. Nucl. Energy*, **82**, pp.47-63 (2002).
34. H. D. Fisher and H. Finnemann, "The Nodal Integration Method – A Diverse Solver for Neutron Diffusion Problems," *Atomkernergie/Kerntechnik*, **39**, pp.229-235 (1981).